JACS
JOURNAL OF THE AMERICAN CHEMICAL SOCIETY

ARTICLE

pubs.acs.org/JACS

Catalytic Mechanism of Water Oxidation with Single-Site Ruthenium−Heteropolytungstate Complexes

Masato Murakami,[†] Dachao Hong,[†] Tomoyoshi Suenobu,[†] Satoru Yamaguchi,[‡] Takashi Ogura,[‡] and Shunichi Fukuzumi*[,†,§]

[†]Department of Material and Life Science, Graduate School of Engineering, Osaka University, ALCA, Japan Science and Technology Agency (JST), Suita, Osaka 565-0871, Japan

[‡]Picobiology Institute, Graduate School of Life Science, University of Hyogo, Hyogo 678-1297, Japan

[§]Department of Bioinspired Science, Ewha Womans University, Seoul 120-750, Korea

Supporting Information

ABSTRACT: Catalytic water oxidation to generate oxygen was achieved using all-inorganic mononuclear ruthenium complexes bearing Keggin-type lacunary heteropolytungstate, $[Ru^{III}(H_2O)SiW_{11}O_{39}]^{5-}$ (**1**) and $[Ru^{III}(H_2O)GeW_{11}O_{39}]^{5-}$ (**2**), as catalysts with $(NH_4)_2[Ce^{IV}(NO_3)_6]$ (CAN) as a one-electron oxidant in water. The oxygen atoms of evolved oxygen come from water as confirmed by isotope-labeled experiments. Cyclic voltammetric measurements of **1** and **2** at various pH's indicate that both complexes **1** and **2** exhibit three one-electron redox couples based on ruthenium center. The Pourbaix diagrams (plots of $E_{1/2}$ vs pH) support that the Ru(III) complexes are oxidized to the Ru(V)−oxo complexes with CAN. The Ru(V)−oxo complex derived from **1** was detected by UV−visible absorption, EPR, and resonance Raman measurements in situ as an active species during the water oxidation reaction. This indicates that the Ru(V)−oxo complex is involved in the rate-determining step of the catalytic cycle of water oxidation. The overall catalytic mechanism of water oxidation was revealed on the basis of the kinetic analysis and detection of the catalytic intermediates. Complex **2** exhibited a higher catalytic reactivity for the water oxidation with CAN than did complex **1**.

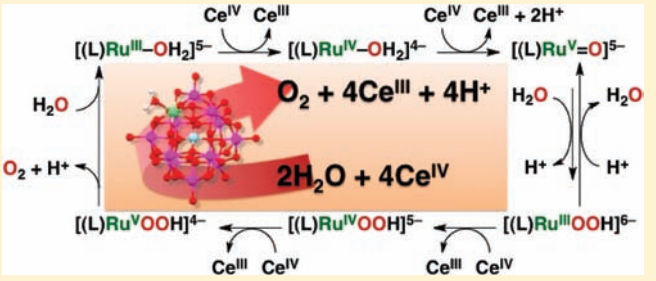

INTRODUCTION

Effective and sustained catalysts for water oxidation are absolutely imperative to achieve the conversion of sunlight into clean and accumulable chemical energy by artificial photosynthesis as typified by sunlight-driven water splitting into hydrogen and oxygen (eqs 1, 2).[1] Thus, extensive efforts have so far been devoted to the development of water oxidation catalysts (WOCs) over the past three decades.[2−4]

$$2H_2O \rightarrow O_2 + 4H^+ + 4e^- \quad (1)$$

$$4H^+ + 4e^- \rightarrow 2H_2 \quad (2)$$

WOCs can be classified into heterogeneous[2] and homogeneous[3,4] types. Heterogeneous WOCs are generally robust and easy to fabricate, providing potential applications. However, the difficulty to identify the catalytically active species of heterogeneous catalysts has precluded clarifying the catalytic mechanism of water oxidation.[2,5] In contrast to heterogeneous catalysts, homogeneous catalysts provide the better opportunity to study the catalytic mechanism of water oxidation, which has yet to be clarified.

The first homogeneous WOC reported by Meyer et al.[6−8] is *cis,cis*-$[(bpy)_2(H_2O)Ru^{III}ORu^{III}(H_2O)(bpy)_2]^{4+}$ (bpy = 2,2′-bipyridine), so-called "blue dimer". To date, several bimetallic Ru[9−19] and Mn[20,21] WOCs have been documented, and the multinuclear structure similar to that in the oxygen evolving complex (OEC) in Photosystem II[22] was regarded to be essential for mediating four-electron process of water oxidation. However, a number of mononuclear Ru[23−34] and Ir[35,36] complexes have also been reported as efficient WOCs. Although the catalytic mechanisms of multinuclear WOCs as the functional model of OEC have attracted considerable attention, there are a few detailed mechanistic studies on binuclear Ru complexes due presumably to the complexity of multinuclear catalysis.[7,11,16,37] Mononuclear WOCs may be more suitable to elucidate the catalytic mechanism of water oxidation because of their simple structure. However, all of the single-site Ru complexes reported so far contain organic ligands,[23−34] and oxidation of the organic ligands under the water oxidation conditions would make it difficult to obtain mechanistic insight into the catalytic water oxidation. To avoid the oxidative damage of WOCs, the adoption

Received: April 6, 2011
Published: June 24, 2011

dx.doi.org/10.1021/ja2024965 | *J. Am. Chem. Soc.* 2011, 133, 11605–11613

Chart 1. Structures of Polyanions 1 and 2[a,44]

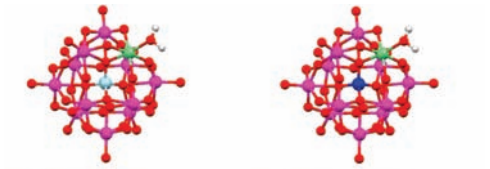

$[Ru^{III}(H_2O)SiW_{11}O_{39}]^{5-}$ (1) $[Ru^{III}(H_2O)GeW_{11}O_{39}]^{5-}$ (2)

[a]Ru, light green; W, purple; O, red; H, white; Si, light blue; Ge, deep blue.

of inorganic ligands, which is stable under water oxidation conditions, is suitable as demonstrated by a tetraruthenium complex with silicodecatungstate $[\{Ru_4O_4(OH)_2(H_2O)_4\}(\gamma\text{-}SiW_{10}O_{36})_2]^{10-}$, which acts a robust water oxidation catalyst with one-electron oxidants such as diammonium cerium(IV) nitrate, $(NH_4)_2[Ce^{IV}(NO_3)_6]$ (CAN), and $[Ru(bpy)_3]^{3+}$ (bpy = 2,2′-bipyridine).[38−41] A tetracobalt complex with phosphononatungstate $[Co_4(H_2O)_2(PW_9O_{34})_2]^{10-}$ was also reported to be capable of oxidizing water with $[Ru^{III}(bpy)_3]^{3+}$.[42,43] However, the catalytic mechanism of water oxidation with those all-inorganic tetranuclear complexes has yet to be clarified, and there has so far been no report on all-inorganic single-site WOCs.

We report herein that single-site ruthenium complexes with heteroundecatungstate, $[Ru^{III}(H_2O)SiW_{11}O_{39}]^{5-}$ (**1**)[44] and $[Ru^{III}(H_2O)GeW_{11}O_{39}]^{5-}$ (**2**) (Chart 1), act as robust water oxidation catalysts with CAN. The catalytic mechanism of water oxidation with **1** and **2** was revealed by electrochemical and spectroscopic measurements as well as by the kinetic analysis. The comparison of the catalytic reactivity between **1** and **2** for water oxidation with CAN provides a valuable insight into the further improvement of the catalytic reactivity for water oxidation.

EXPERIMENTAL SECTION

Materials. $Cs_5[Ru^{III}(H_2O)SiW_{11}O_{39}]$ (Cs_5·**1**) and $Cs_5[Ru^{III}(H_2O)GeW_{11}O_{39}]$ (Cs_5·**2**) were prepared according to the literature procedures and characterized by IR, UV−visible spectroscopic, and electrochemical measurements.[44] Commercially available reagents, sodium sulfate (Na_2SO_4), phosphoric acid (H_3PO_4), boric acid (H_3BO_4), acetic acid (CH_3COOH), nitric acid (HNO_3), diluted nitric acid (1.0 and 0.1 M HNO_3), diammonium cerium(IV) nitrate ($(NH_4)_2[Ce^{IV}(NO_3)_6]$, CAN), diammonium cerium(III) nitrate ($(NH_4)_2[Ce^{III}(NO_3)_5]$) (Wako Pure Chemical Industries), D_2O (99.9% D), and $H_2{}^{18}O$ (97% ^{18}O) (Cambridge Isotope Laboratories), were used without further purification.

General Methods. Purification of water (18.2 MΩ cm) was performed with a Milli-Q system (Millipore, Direct-Q 3 UV). UV−visible absorption spectra were recorded using a Hewlett-Packard 8453 diode array spectrophotometer with a quartz cuvette (the light path length = 1 cm). The pH values of a solution were determined by a pH meter (TOA, HM-20J) equipped with a pH combination electrode (TOA, GST-5725C). The pH meter was calibrated relative to standard phthalate (pH 4.0) and phosphate (pH 6.9) buffer solutions prior to each use.

TGA Analysis. The number of crystal waters in **1** and **2** were determined to be 6 and 8, respectively, based on the results of TGA analysis recorded on an SII TG/DTA 7200 instrument. The samples (∼5 mg) were heated from 25 to 300 °C with a ramp rate of 2 °C/min. The number of crystal water contained in the sample was evaluated from the weight loss by heating the sample.

Catalytic Oxygen Evolution. The yield of oxygen was determined with a Shimadzu GC-17A gas chromatograph {Ar carrier, a capillary column with molecular sieves (Agilent Technologies, 19095P-MS0, 30 m × 0.53 mm) at 313 K} equipped with a thermal conductivity detector. An aliquot (100 μL) of a deaerated 0.1 M HNO_3 aqueous solution containing **1** (6.0×10^{-7} mol) was injected into a deaerated 0.1 M HNO_3 aqueous solution (2 mL) containing CAN (1.2×10^{-5} mol) in the reaction vessel (4.9 mL) with a magnetic stirrer. At every 10 min, 100 μL of gas in headspace of the reaction vessel was taken using a gastight syringe and analyzed by GC. The total amount of evolved oxygen was determined on the basis of the calibration curve prepared for various concentrations of oxygen in argon gas.

Isotope-Labeled Experiment. The ratio of $^{16}O_2$, $^{16}O^{18}O$, and $^{18}O_2$ was determined on the basis of the intensity of mass spectrum (m/z = 32, 34, and 36) obtained on a Shimadzu GC-17A gas chromatograph {He carrier, TC-FFAP column (GL Science, 1010-15242) at 313 K} equipped with a mass spectrometer (Shimadzu, QP-5000). An aliquot (100 μL) of a deaerated $H_2{}^{18}O$ solution (83.8% ^{18}O) containing **1** (3.0×10^{-7} mol) and HNO_3 (0.1 M) was injected to into 1 mL of a deaerated $H_2{}^{18}O$ solution (83.8% ^{18}O) containing CAN (6.0×10^{-6} mol) and HNO_3 (0.1 M) in the reaction vessel (2 mL). The air in the headspace of sealed reaction vessel was replaced by He before the reaction by bubbling He gas through syringe. After 1 h, 50 μL of gas in headspace of the reaction vessel was taken using a gastight syringe and analyzed by GC−MS.

Determination of pK_a Values. The spectroscopic titrations were performed to determine the pK_a values of **1** and **2** in a 0.1 M Britton−Robinson buffer ($[CH_3COOH]$ = 0.1 M, $[H_3PO_4]$ = 0.1 M, $[H_3BO_4]$ = 0.1 M) at 298 K. A small amount of 0.36−3.6 M NaOH aqueous solutions was added to a 0.1 M Britton−Robinson buffer solution containing **1** (5.0×10^{-4} M) or **2** (5.0×10^{-4} M). The absorption spectra of **1** and **2** were changed with an increase in pH, and the plot of absorbance at particular wavelengths (λ = 440 nm for **1**, λ = 430 nm for **2**) versus pH was fitted by eq 3:

$$A = A_0 + K_a(A_\infty - A_0)/(K_a + 10^{-pH}) \quad (3)$$

where A_0 is the absorbance of the aqua complex, and A_∞ is the absorbance of the hydroxo complex. The pK_a value was determined from the fitting curve as the pH value when the absorbance was the average value of A_0 and A_∞. Derivation of eq 3 is described in the Supporting Information.

Electrochemical Measurements. Cyclic voltammetry (CV) was performed on an ALS 630B electrochemical analyzer using a glassy carbon electrode as a working electrode, a saturated calomel electrode (SCE) as a reference electrode, and Pt wire as an auxiliary electrode. Cyclic voltammograms and differential pulse voltammograms of **1** (2.0×10^{-3} M) and **2** (2.0×10^{-3} M) were obtained in 0.1 M Britton−Robinson buffer solutions in the range of 1.5 < pH < 8.0 and in 0.1 M Na_2SO_4 aqueous solutions in the range of 0 < pH < 1.5. The pH of a solution was changed by using 0.36−3.6 M NaOH aqueous solutions and HNO_3 (69%).

Spectral Titration. The UV−visible spectroscopic titration was performed with a spectrophotometer. UV−visible spectra were taken after every addition of a 0.1 M HNO_3 aqueous solution (20 μL) containing CAN (6.0×10^{-3} M) to a 0.1 M HNO_3 aqueous solution (2 mL) containing **1** (3.0×10^{-4} M). The absorbances at λ = 380 and 550 nm were plotted against the ratio of [CAN] to [**1**].

Electron Paramagnetic Resonance (EPR) Measurements. The EPR cell (3.0 mm i.d.) containing a deaerated 0.1 M HNO_3 aqueous solution (0.5 mL) of **1** (1.0×10^{-3} M) or **2** (1.0×10^{-3} M) was maintained at 77 K in a liquid-nitrogen dewar. The remaining gas in headspace of the EPR cell was removed under vacuum, and then the EPR cell was cooled to 4 K with use of liquid helium in the EPR cavity and EPR spectrum was taken on a JEOL JEX-REIXE spectrometer under

nonsaturating microwave power conditions. The magnitude of the modulation was chosen to optimize the resolution and the signal-to-noise (S/N) ratio of the observed spectra. The g values were calibrated using Mn^{2+} marker. The EPR spectrum of oxidized **1** was obtained as follows. A deaerated 0.1 M HNO_3 aqueous solution (0.5 mL) of **1** (1.0×10^{-3} M) and a deaerated 0.1 M HNO_3 aqueous solution (10 μL) of CAN were mixed in an EPR cell. After a few seconds, the EPR cell was cooled to 77 K in a liquid-nitrogen Dewar, and the remaining gas in headspace of the EPR cell was removed under vacuum. The EPR spectrum of the mixture was measured after cooling the EPR cell at 4 or 77 K. The EPR spectrum of oxidized **2** was measured in the same manner as that of **1**.

Resonance Raman (rR) Measurements. RR spectra were measured using a λ 442 nm line of a HeCd laser (Kinmon, IK4401R-D). The laser power at the sample point was 10 mW. The sample solution was in an NMR tube and spun with a spinning cell device designed to minimize off-center deviation during rotation. Raman scattered light was collected at 135° with a pair of fused quartz lenses, f-matched to a 1.0 m spectrograph (Ritsu Oyo Kogaku, MC-1000DG), which was equipped with a holographic grating (2400 grooves mm^{-1}) and a liquid nitrogen-cooled CCD detector. A depolarizer was used to scramble the polarization of collected light and thus eliminate intensity artifacts created by polarization-dependent grating reflectivity. The spectra were calibrated using the standard Raman spectra of acetone and indene. An aliquot (10 μL) of an $H_2{}^{16}O$ or $H_2{}^{18}O$ solution of CAN (1.5×10^{-6} mol) was added to a 500 μL $H_2{}^{16}O$ or $H_2{}^{18}O$ solution of **1** (5.0×10^{-7} mol) and **2** (5.0×10^{-7} mol). Formation of a precipitate was observed immediately after mixing two solutions of **1** (or **2**) and CAN. The precipitate was removed with a membrane filter and the filtrate was transferred to a quartz NMR tube, and then the NMR tube was supplied for rR measurement.

Kinetic Measurements. All kinetic experiments were performed using a spectrophotometer with 1 cm cell at 298 K. The absorbance at λ = 420 nm assignable to CAN was monitored during water-oxidation reaction under various conditions. Each of initial reaction rates was obtained on the basis of the decay rate of absorbance at λ = 420 nm.

RESULTS AND DISCUSSION

Catalytic Water Oxidation. The catalytic water oxidation was investigated by an addition of 20 equiv of Ce^{IV} to an aqueous solution containing **1** (3.0×10^{-4} M) and 0.1 M HNO_3, and the evolution of oxygen was confirmed by gas-chromatographic analysis (see Experimental Section and Figure S1 in the Supporting Information). The loss of Ce^{IV} was monitored by a photodiode array UV−visible spectrophotometer (λ = 400 nm), and the amount of evolved O_2 was determined by gas chromatography. The result of a typical experiment is shown as the time profiles of the decay of Ce^{IV} and the evolution of O_2 in Figure 1a. The decrease in the concentration of CAN in the solution virtually coincides with the O_2 evolution (Figure 1b), and 2.7 μmol of oxygen was finally produced from 12 μmol of CAN. The efficiency of oxygen evolution is approximately 90% based on the initial amount of oxidant, indicating that nearly stoichiometric water oxidation by Ce^{IV} occurred with **1**; that is, 4 equiv of Ce^{IV} is consumed for 1 equiv of O_2 evolution based on eq 1. TONs of oxygen evolution catalyzed by **1** and **2** reach up to 20 and 50, respectively.

The oxygen evolution was not observed upon additions of $RuCl_3 \cdot 3H_2O$, $Ru(acac)_3$, and $K_8[SiW_{11}O_{39}]$ instead of **1** to an aqueous solution containing CAN and 0.1 M HNO_3. The addition of **2** to the same aqueous solution led to more efficient oxygen evolution as compared to **1**. Thus, it should be noted that only **1** and **2** were able to act as a water oxidation catalyst with CAN, and the ruthenium sources and the ruthenium-free ligand of **1** had no effect on the catalysis.

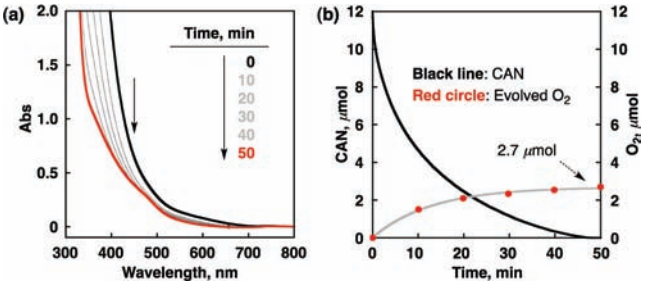

Figure 1. (a) UV−vis spectral changes in the course of the reaction of **1** (3.0×10^{-4} M) with CAN (6.0×10^{-3} M) in 0.1 M HNO_3 at 298 K. (b) Time course of the amount of evolved oxygen (red ●) and CAN (−) in the reaction of **1** (3.0×10^{-4} M) with CAN (6.0×10^{-3} M) in 0.1 M HNO_3 at 298 K.

Table 1. Observed and Theoretical Relative Abundances of ^{18}O-Labeled and Unlabeled Oxygen Evolved during the Oxidation of $H_2{}^{18}O$-Enriched Water (83.8% $H_2{}^{18}O$) Catalyzed by 1 (3.0×10^{-4} M) with CAN (6.0×10^{-3} M) in 0.1 M HNO_3 at 298 K

	relative abundance, %		
	$^{16}O_2$	$^{16}O^{18}O$	$^{18}O_2$
observed	3.4	26.7	69.9
theoretical[a]	2.6	27.2	70.2

[a] Theoretical values were calculated by assuming that evolved oxygen comes only from water.

We conducted GC−MS analysis of oxygen evolved during water oxidation using $H_2{}^{18}O$ to clarify the oxygen source of evolved oxygen. The evolved oxygen in the oxidation of water with CAN in $H_2{}^{18}O$-enriched aqueous solution (83.8% ^{18}O) containing **1** and 0.1 M HNO_3 was analyzed by GC−MS (Figure S2 in the Supporting Information). In the mass spectrum, the molecular ion peak at m/z = 36 assignable to $^{18}O_2$ exhibited the largest intensity among the molecular ion peaks at m/z = 32, 34, and 36 (Table S1 in the Supporting Information). The relative abundance of oxygen isotopes, which were determined from the intensities of those three molecular ion peaks, is listed in Table 1. The theoretical ratio of oxygen isotopes in Table 1 was calculated by assuming that both oxygen atoms of oxygen come only from water. The observed ratios agree well with the calculated ratios, indicating that evolved oxygen comes exclusively from water.

Redox Properties of 1 and 2. To get insight into the catalytically active species for water oxidation with CAN, we have examined the comprehensive redox and acid−base properties of **1** and **2** by electrochemical and pK_a measurements. The electrochemical behavior and the pK_a values of **1** and **2** were studied in a broad pH range. The aqua complexes **1** and **2** are converted to the corresponding hydroxo complexes, that is, $(L)Ru^{III}-OH$ (L = $[SiW_{11}O_{39}]^{8-}$ for **1** or $[GeW_{11}O_{39}]^{8-}$ for **2**) by increasing pH as shown in Figure 2. The pK_a values of the aqua complexes of **1** and **2** are determined by fitting eq 3 (Experimental Section) to the data of UV−visible spectroscopic titration in Figure 2 to be 6.4 and 6.2, respectively.

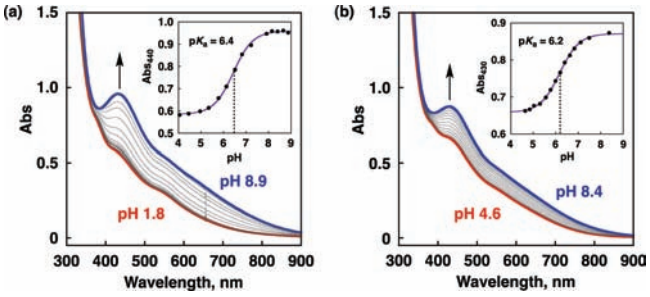

Figure 2. Absorption spectral changes in the course of titration of (a) **1** (5.0×10^{-4} M) and (b) **2** (5.0×10^{-4} M) with NaOH aqueous solution in 0.1 M Britton−Robinson buffer at 298 K. Inset: Plot of the absorbance at λ = 440 nm for **1** and λ = 430 nm for **2** versus pH.

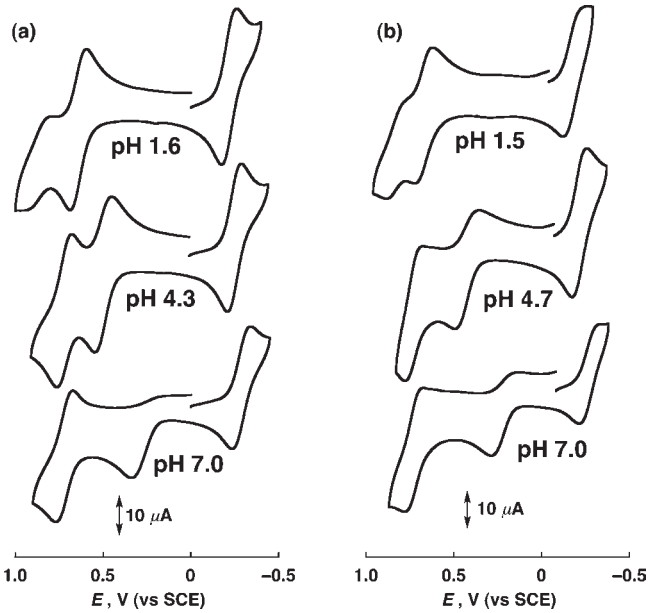

Figure 3. Cyclic voltammograms of (a) $[Ru^{III}SiW_{11}O_{39}]^{5-}$ (**1**, 2.0×10^{-3} M) and (b) $[Ru^{III}GeW_{11}O_{39}]^{5-}$ (**2**, 2.0×10^{-3} M) depending on pH with a scan rate of 0.1 V/s in 0.1 M Britton−Robinson buffer at 298 K. The pH of the solution was adjusted by NaOH aqueous solution.

Cyclic voltammograms of **1** and **2** depending on pH were measured in the range of 0 < pH < 8 (Figure 4).[45] Both **1** and **2** undergo three one-electron oxidation processes, each of which exhibited ca. 90 mV of a peak separation at a sweep rate of 0.1 V s^{-1}, indicating that three one-electron redox couples are chemically reversible. The first one-electron reduction process starting from the Ru(III) complexes is ascribed to the Ru(III)/Ru(II) redox couple, whereas the first and second one-electron oxidation processes are ascribed to the Ru(IV)/Ru(III) and Ru(V)/Ru(IV) redox couples, respectively. The three one-electron redox potentials are shifted to a positive direction with decreasing pH (Figure 3).[46]

Figure 4 illustrates the Pourbaix diagrams ($E_{1/2}$ vs pH)[47] for **1** and **2** in the range of 0 < pH < 8 in water. When $E_{1/2}$ is independent of pH, no proton is coupled in the one-electron redox process.[44a,48] On the other hand, when $E_{1/2}$ decreases with increasing pH with a slope of 59 and 118 mV, one and two protons are coupled with the one-electron redox process, respectively.[47]

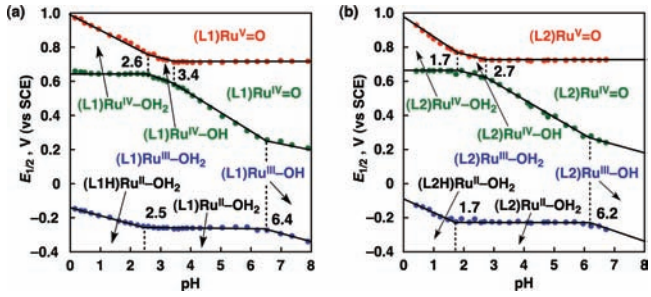

Figure 4. Pourbaix diagrams for (a) **1** and (b) **2**. The blue, green, and red points correspond to the Ru(III)/Ru(II), Ru(IV)/Ru(III), and Ru(V)/Ru(IV) redox potentials, respectively. All four pK_a values are shown by the vertical dashed lines. L1 and L2 denote the ligand of **1** and **2**, respectively.

Thus, all of the species depending on the $E_{1/2}$ and pH values can be identified as shown in Figure 4. For example, the $(L)Ru^{III}-OH_2$ (L = $[SiW_{11}O_{39}]^{8-}$ for **1** or $[GeW_{11}O_{39}]^{8-}$ for **2**) complex is oxidized to the $(L)Ru^{IV}-OH_2$ complex at pH 1 at an applied potential between 0.62 and 0.90 V (vs SCE) without losing proton when the $E_{1/2}$ value remains constant with the change in pH around 1. In contrast, the $(L)Ru^{IV}-OH_2$ complex is oxidized to the $(L)Ru^{V}=O$ complex at pH 1 at an applied potential above 0.90 V with removal of two protons, when the $E_{1/2}$ value decreases with increasing pH from 1 with a slope of 118 mV. Thus, **1** and **2** are expected to be oxidized by CAN ($E_{1/2}$ = 1.21 V vs SCE at pH 1.0,[34b] and $E_{1/2}$ = 1.61 V vs NHE (= 1.34 V vs SCE) at lower pH with 0.5−5 M HNO_3)[34c] to the $(L)Ru^{V}=O$ complexes of **1** and **2**, respectively. The complexes **1** and **2** are not stable at pH higher than 8.

All four pK_a values of **2** (6.2 for $[Ru^{III}(H_2O)GeW_{11}O_{39}]^{5-}$, 1.7 for $[Ru^{II}(H_2O)HGeW_{11}O_{39}]^{5-}$, 2.7 for $[Ru^{IV}(H_2O)GeW_{11}O_{39}]^{4-}$, and 1.7 for $[Ru^{IV}(OH)GeW_{11}O_{39}]^{5-}$) are smaller than the corresponding values of **1** (6.4 for $[Ru^{III}(H_2O)SiW_{11}O_{39}]^{5-}$, 2.5 for $[Ru^{II}(H_2O)HSiW_{11}O_{39}]^{5-}$, 3.4 for $[Ru^{IV}(H_2O)SiW_{11}O_{39}]^{4-}$, and 2.6 for $[Ru^{IV}(OH)SiW_{11}O_{39}]^{5-}$). This indicates that the ruthenium site and the ligand of **2** are more difficult to be protonated due to the electron-withdrawing effect of germanium, core-atom of the ligand, because of the larger electronegativity of germanium (2.01) than silicon (1.90).[49] The Ge that is more electronegative than Si withdraws electron at higher degree from the framework of polytungstate anion, which causes the lower basicity of the heteropolytungstate anion. The weaker coordination of the heteropolytungstate anion resulted in the higher acidity of the Ru metal center, which induces the higher acidity of the coordinated aqua ligand with lower pK_a.

Spectroscopic Redox Titrations. The UV−visible spectral titration of **1** with CAN in an acidic medium showed that the oxidation of **1** led to the formation of corresponding Ru(IV) and Ru(V) complexes as shown in Figure 5. The formation of respective Ru(IV) and Ru(V) species was observed with the isosbestic points (λ = 500 nm for first one-electron oxidation, λ = 358, 500 nm for second one-electron oxidation) by adding stoichiometric equivalents of CAN to aqueous solution containing **1** (3.0×10^{-4} M) and 0.1 M HNO_3. According to the Pourbaix diagram for **1** in Figure 4a, the respective Ru(IV) and Ru(V) species in the range of 0 < pH < 2.6 can be assigned to $[Ru^{IV}(H_2O)SiW_{11}O_{39}]^{4-}$ and $[Ru^{V}(O)SiW_{11}O_{39}]^{5-}$. The first and second electron-transfer processes between **1** and CAN are thermodynamically favorable due to the high reduction potential

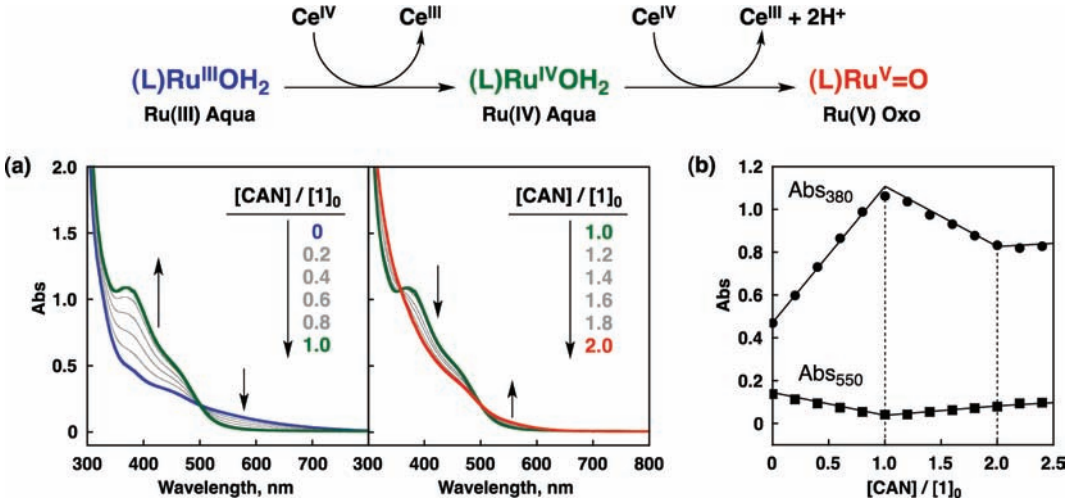

Figure 5. (a) UV−visible spectral changes of **1** upon addition of CAN in 0.1 M HNO_3 at 298 K. The initial concentration of **1**, $[\mathbf{1}]_0$, was 3.0×10^{-4} M. Each spectrum was monitored after every addition of 0.2 equiv of CAN. (b) Plots of the absorbance at $\lambda = 380$ (●) and 550 nm (■) relative to the ratio of [CAN] to $[\mathbf{1}]_0$.

of Ce(IV)/Ce(III), which is 1.61 V vs NHE (1.34 V vs SCE).[34c] Because the oxidation potentials of $[Ru^{III}(H_2O)SiW_{11}O_{39}]^{5-}$ and $[Ru^{IV}(H_2O)SiW_{11}O_{39}]^{4-}$ at pH 1.0 were determined to be 0.64 and 0.91 V, respectively, the reduction potential of CAN is high enough to oxidize these complexes under the catalytic conditions. The driving forces of the first and second electron-transfer processes are estimated to be 0.57 and 0.30 eV, respectively. Thus, the first and second electron-transfer oxidation processes are expected to proceed at the diffusion-limited rate. Actually, the rates of electron-transfer oxidation of **1** and **2** with CAN were too fast to be determined even by using a stopped-flow method. This indicates that the electron-transfer rate constant is larger than 10^6 M^{-1} s^{-1}.[50]

In cryogenic EPR measurements at 4 K, **1** exhibited a two-axis anisotropic signal with $g_\perp = 2.4$ and $g_\parallel = 2.0$ (Figure 6a). The spin state of **1** can be assigned to $S = 1/2$, and the oxidation number of ruthenium in **1** is III judging from the $g_\perp$ value higher than 2.3.[51] The addition of 2 equiv of CAN to the solution of **1** resulted in a sharp two-axis anisotropic signal at $g_\perp = 2.1$ and $g_\parallel = 1.9$ (Figure 6b) at 77 K. This indicates that the spin state of **1** under catalytic conditions is also $S = 1/2$. The anisotropic EPR signal at $g_\perp = 2.1$ and $g_\parallel = 1.9-2.0$ is not characteristic of the Ru^{III} species, but the Ru^V═O species as reported in the literature.[51,52] On the other hand, the EPR signal due to Ce^{III} ion observable at 4 K (Figure S4) was not observed at 77 K due to the strong spin−orbit coupling and the short relaxation time of the $4f^1$ state above 30 K.[53] Thus, these EPR results together with rR spectral data (vide infra) rationalize the steady state formation of $[(L)Ru^V{=}O]^{5-}$ of **1** in the catalytic cycle. In the case of **2**, the EPR spectra of **2** and its oxidized species showed tendency similar to those of complex **1**; see Figure S3 in the Supporting Information.

The characterization of the catalytically active species derived from **1** for water oxidation was also performed by the resonance Raman (rR) measurements. Figure 7 shows the result of the rR measurements of oxidized **1** produced by the addition of CAN (3 equiv, 3.0×10^{-3} M) in water with excitation at $\lambda = 442$ nm. The Raman scattering at 800 cm^{-1} was observed, and this was shifted to 785 cm^{-1} when $H_2{}^{18}O$ was employed as a solvent. Similar Raman bands were observed for oxidized **2** with CAN

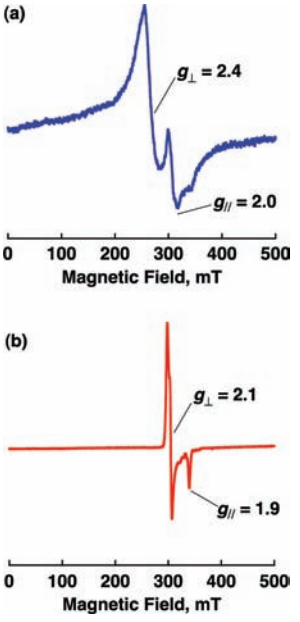

Figure 6. (a) X-band EPR spectrum of **1** (1.0×10^{-3} M) measured at 4 K in a frozen 0.1 M HNO_3 solution. (b) X-band EPR spectrum of **1** (1.0×10^{-3} M) observed upon addition of 2 equiv of CAN to a 0.10 M HNO_3 solution measured at 77 K. The scale in longitudinal axis of (b) is 15 times larger than that of (a).

(Figure S5 in the Supporting Information). The rR band appearing at 800 cm^{-1} is assignable to the typical Ru^V═O species as identified in the previous papers.[54,55] In comparison with other Ru═O complexes together with the results of the redox titration and the EPR spectrum, this band is assigned to the stretching of the Ru(V)−oxo double bond (Ru^V═O) of $[Ru^V(O)SiW_{11}O_{39}]^{5-}$. The smaller isotopic shift (15 cm^{-1}) than the theoretical value for the ^{18}O substitution in a Ru═O harmonic oscillator ($\Delta\nu = 40$ cm^{-1}) may result from the binding of Ce(IV) to the oxo complex as suggested by the literature.[55]

The UV−visible spectrum of **1** observed during the catalytic oxidation with CAN in an aqueous solution containing 0.1 M

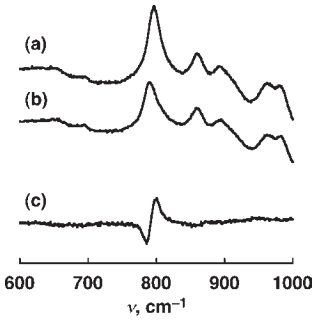

Figure 7. (a) Resonance Raman spectrum of $[Ru^{V}(^{16}O)SiW_{11}O_{39}]^{5-}$ generated in the reaction of $[Ru^{III}(H_2{}^{16}O)SiW_{11}O_{39}]^{5-}$ with CAN in $H_2{}^{16}O$ solution at room temperature with an excitation wavelength of λ = 442 nm. (b) Resonance Raman spectrum of $[Ru^{V}(^{18}O)SiW_{11}O_{39}]^{5-}$ generated in the reaction of $[Ru^{III}(H_2{}^{18}O)SiW_{11}O_{39}]^{5-}$ with CAN in $H_2{}^{18}O$ solution at room temperature with an excitation wavelength of λ = 442 nm. (c) Difference spectrum between (a) and (b).

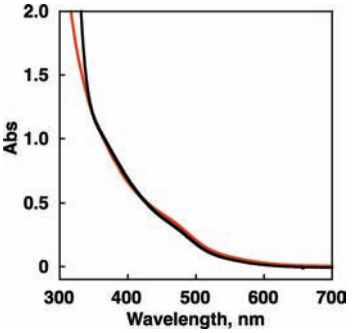

Figure 8. UV−vis absorption spectrum of **1** (3.0×10^{-4} M) during water oxidation (black) and that of $[Ru^{V}(O)SiW_{11}O_{39}]^{5-}$ (3.0×10^{-4} M) obtained by the titration with CAN as shown in Figure 5a (red).

HNO_3 (Figure 8) agrees well with the spectrum of $[Ru^{V}(O)SiW_{11}O_{39}]^{5-}$ in Figure 5a. Because the formation of $[Ru^{V}(O)SiW_{11}O_{39}]^{5-}$ by the electron-transfer oxidation of **1** with CAN is very fast (vide supra), the Ru^{V}=O complex remains the catalytically active species for the water oxidation. The more detailed mechanistic insight is provided by the kinetic analysis (vide infra).

Kinetics and Catalytic Mechanism. Kinetic studies on the catalytic oxidation of water by CAN with **1** and **2** were conducted with an excess amount of CAN in acidic media to clarify the catalytic mechanism. The rates of water oxidation were determined from the decay rates of CAN, which agree with the rates of oxygen evolution (see Figure 1b). The decay rate of CAN was determined by monitoring the decay of absorbance at λ = 400 and 420 nm due to CAN using a photodiode array UV−visible spectrophotometer (see Experimental Section). The initial rates of water oxidation (R_i) were used to analyze the kinetics under catalytic turnover conditions to avoid the effect of decomposition of **1** and **2** under strongly acidic conditions.

The initial rates of water oxidation were investigated with various concentrations of **1** and **2** in an aqueous solution containing 100 equiv of CAN and 0.55 M HNO_3.[56] The relatively high concentration of HNO_3, that is, 0.55 M, was employed because the solubility of catalyst **2** was limited in the presence of

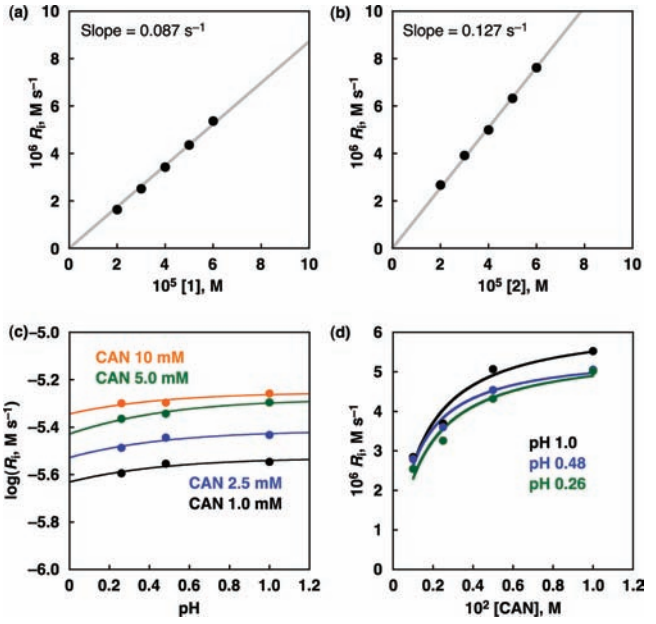

Figure 9. (a) Dependence of the initial rate (R_i) on [**1**] in the water oxidation catalyzed by **1** with CAN (100 equiv, $(2.0-6.0) \times 10^{-3}$ M) in 0.55 M HNO_3 at 298 K. (b) Dependence of R_i on [**2**] in the water oxidation catalyzed by **2** with CAN (100 equiv, $(2.0-6.0) \times 10^{-3}$ M) in 0.55 M HNO_3 at 298 K. (c) Dependence of log R_i on pH in the water oxidation catalyzed by **1** (5.0×10^{-5} M) with CAN ($(0.10-1.0) \times 10^{-2}$ M) in 0.10−0.55 M HNO_3 at 298 K. (d) Dependence of R_i on [CAN] in the water oxidation catalyzed by **1** (5.0×10^{-5} M) with CAN ($(0.10-1.0) \times 10^{-2}$ M) in 0.10−0.55 M HNO_3 at 298 K.

CAN at higher pH in the presence of 0.1 M HNO_3 due to the countercation exchange. The rate law is determined to be first order with respect to the concentrations of **1** and **2** as shown in Figure 9a and b, respectively. If two Ru^{V}=O molecules, that is, two $[Ru^{V}(O)SiW_{11}O_{39}]^{5-}$ for **1** or two $[Ru^{V}(O)GeW_{11}O_{39}]^{5-}$ for **2**, are involved for O−O bond formation in O_2 evolution, the rate law would be second order with respect to the catalyst concentration. Thus, the most likely reaction pathway for the O−O bond formation may be the reaction of the Ru^{V}=O complex with water to produce the Ru^{III}−OOH complex.[23,24] The water oxidation rate slightly increases with increasing pH (Figure 9c), and it also increases with increasing concentration of CAN to approach a constant value (Figure 9d). If the reaction of the Ru^{V}=O complex with water is solely the rate-determining step for the water oxidation, the water oxidation rate would be constant with change in pH or concentrations of CAN, because the formation of the Ru^{V}=O complex by the electron-transfer oxidation of **1** with CAN occurs at the diffusion-limited rate (vide supra). The saturation behaviors of the water oxidation rate with increasing pH and concentration of CAN indicate that the subsequent oxidation of the Ru^{III}−OOH complex by CAN competes with the back reaction from the Ru^{III}−OOH complex, which undergoes the O−O bond cleavage to regenerate the Ru^{V}=O complex as shown in Scheme 1. The driving force of dissociation of H^+ and O_2 from $[(L)Ru^{V}-OOH]^{4-}$ could be attributed to the deprotonation coupled with the oxidation of the peroxo ligand ($O_2{}^{2-}$) with high valent Ru^{V}. This may be the reason why the deprotonation occurs in such a highly acidic medium.

Scheme 1

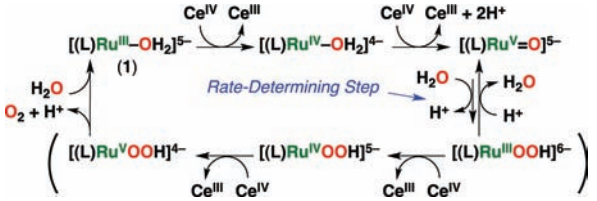

According to Scheme 1, the water oxidation rate (R_i) is given by eq 4:

$$R_i = k_w k_{et}[Ru^V{=}O][H_2O][CAN]/(k_{-w}[H^+] + k_{et}[CAN]) \quad (4)$$

where k_w is the rate constant of the reaction of the $Ru^V{=}O$ complex with H_2O to produce the $Ru^{III}-OOH$ complex, k_{et} is the rate constant of electron transfer from the $Ru^{III}-OOH$ complex to CAN, and k_{-w} is the rate constant of the back reaction from the $Ru^{III}-OOH$ complex with H^+ to regenerate the $Ru^V{=}O$ complex. Equation 4 agrees with experimental observations in Figure 9: the first-order dependence on the catalyst concentration that corresponds to $[Ru^V{=}O]$, the saturation dependence on pH, and the CAN concentration. Thus, the catalytic water oxidation by CAN with the $Ru^{III}-OH_2$ complex (**1** and **2**) proceeds via the $Ru^V{=}O$ complex, which is immediately formed by the fast two-electron oxidation of the $Ru^{III}-OH_2$ complex coupled with deprotonation. The reaction of the $Ru^V{=}O$ complex with H_2O to produce the $Ru^{III}-OOH$ complex is the rate-determining step, but the electron transfer oxidation of the $Ru^{III}-OOH$ by CAN leading to the oxygen evolution competes with the back reaction from the $Ru^{III}-OOH$ complex with H^+ to regenerate the $Ru^V{=}O$ complex. Because the further oxidation of the $Ru^{III}OOH$ complex may be fast (not the rate-determining step), the $Ru^{IV}OOH$ intermediate in Scheme 1 is putative.

It should be noted that the rate of **2** (Figure 9b) is 1.5 times higher than that of **1** (Figure 9a). The higher catalytic reactivity of **2** may result from the electron-withdrawing effect of germanium (core atom of the ligand), which are reflected by the smaller pK_a values of **2** as compared to **1** (vide supra).[57] Thus, the present study provides valuable insight into the further improvement of the catalytic reactivity for water oxidation.

CONCLUSIONS

In this study, catalytic water oxidation was demonstrated using two types of all-inorganic mononuclear ruthenium complexes, **1** and **2**. TONs of oxygen evolution catalyzed **1** and **2** reach up to 20 and 50, respectively. The origin of evolved oxygen was revealed to be water by ^{18}O isotope-labeling experiments in $H_2{}^{18}O$, where $^{18}O^{18}O$ was mainly obtained by measuring GC−MS. The intermediate $Ru^V{=}O$ complex of **1** was detected by a characteristic anisotropic EPR signal at $g_\perp = 2.1$ and $g_\parallel = 1.9$ at 77 K and a resonance Raman peak, which show the significant isotopic shift when the measurement has been done in $H_2{}^{18}O$. The $(L)Ru^V{=}O$ complex is the two-electron oxidized species of **1** and **2** assignable to an active intermediate for oxidizing water in the rate-determining step of the whole catalytic cycle to give $(L)Ru^{III}OOH$ via the O−O bond formation step, where the reverse O−O bond cleavage process might be in competition with the follow-up two electron oxidation processes to generate oxygen. Actually the rate-determining equilibrium between $(L)Ru^V{=}O$ and $(L)Ru^{III}OOH$ was confirmed by the observation of saturated dependence of the oxygen evolution rate on pH and the concentration of CAN. When the catalytic reactivity of **1** was compared to that of **2**, the improvement of the catalytic reactivity was made possible by changing the core-atom of the heteropolytungstate ligand from Si to Ge.

ASSOCIATED CONTENT

Supporting Information. Gas chromatograms, GC mass spectrum, table of the relative abundance of oxygen isotopes, EPR spectra, resonance Raman spectra, cyclic voltammograms, derivation of eq 3, and complete ref 41c. This material is available free of charge via the Internet at http://pubs.acs.org.

AUTHOR INFORMATION

Corresponding Author
fukuzumi@chem.eng.osaka-u.ac.jp

ACKNOWLEDGMENT

This work was supported by a Grant-in-Aid (no. 20108010) and a Global COE program, "The Global Education and Research Center for Bio-Environmental Chemistry", from the Ministry of Education, Culture, Sports, Science and Technology, Japan, and also by NRF/MEST through WCU (R31-2008-000-10010-0), Korea.

REFERENCES

(1) (a) Lewis, N. S.; Nocera, D. G. *Proc. Natl. Acad. Sci. U.S.A.* **2006**, *103*, 15729. (b) Fukuzumi, S. *Phys. Chem. Chem. Phys.* **2008**, *10*, 2283. (c) Gray, H. B. *Nat. Chem.* **2009**, *1*, 7. (d) Hurst, J. K. *Science* **2010**, *328*, 315.

(2) (a) Youngblood, W. J.; Lee, S.-H. A.; Maeda, K.; Mallouk, T. E. *Acc. Chem. Res.* **2009**, *42*, 1966. (b) Kanan, M. W.; Surendranath, Y.; Nocera, D. G. *Chem. Soc. Rev.* **2009**, *38*, 109.

(3) (a) Rüttinger, W.; Dismukes, G. C. *Chem. Rev.* **1997**, *97*, 1. (b) Yagi, M.; Kaneko, M. *Chem. Rev.* **2001**, *101*, 21.

(4) (a) Hurst, J. K. *Coord. Chem. Rev.* **2005**, *249*, 313. (b) Cady, C. W.; Crabtree, R. H.; Brudvig, G. W. *Coord. Chem. Rev.* **2008**, *252*, 444. (c) Sala, X.; Romero, I.; Rodríguez, M.; Escriche, L.; Llobet, A. *Angew. Chem., Int. Ed.* **2009**, *48*, 2842. (d) Dismukes, G. C.; Brimblecombe, R.; Felton, G. A. N.; Pryadun, R. S.; Sheats, J. E.; Spiccia, L.; Swiegers, G. F. *Acc. Chem. Res.* **2009**, *42*, 1935. (e) Concepcion, J. J.; Jurss, J. W.; Brennaman, M. K.; Hoertz, P. G.; Patrocinio, A. O. T.; Murakami Iha, N. Y.; Templeton, J. L.; Meyer, T. J. *Acc. Chem. Res.* **2009**, *42*, 1954.

(5) Sala, X.; Ertem, M. Z.; Vigara, L.; Todorova, T. K.; Chen, W.; Rocha, R. C.; Aquilante, F.; Cramer, C. J.; Gagliardi, L.; Llobet, A. *Angew. Chem., Int. Ed.* **2010**, *49*, 7745.

(6) (a) Gersten, S. W.; Samuels, G. J.; Meyer, T. J. *J. Am. Chem. Soc.* **1982**, *104*, 4029. (b) Gilbert, J. A.; Eggleston, D. S.; Murphy, W. R.; Geselowitz, D. A.; Gersten, S. W.; Hodgson, D. J.; Meyer, T. J. *J. Am. Chem. Soc.* **1985**, *107*, 3855. (c) Geselowitz, D.; Meyer, T. J. *Inorg. Chem.* **1990**, *29*, 3894.

(7) (a) Chronister, C. W.; Binstead, R. A.; Ni, J.; Meyer, T. J. *Inorg. Chem.* **1997**, *36*, 3814. (b) Binstead, R. A.; Chronister, C. W.; Ni, J.; Hartshorn, C. M.; Meyer, T. *J. Am. Chem. Soc.* **2000**, *122*, 8464. (c) Liu, F.; Concepcion, J. J.; Jurss, J. W.; Cardolaccia, T.; Templeton, J. L.; Meyer, T. J. *Inorg. Chem.* **2008**, *47*, 1727.

(8) (a) Concepcion, J. J.; Jurss, J. W.; Templeton, J. L.; Meyer, T. J. *Proc. Natl. Acad. Sci. U.S.A.* **2008**, *105*, 17632. (b) Jurss, J. W.; Concepcion, J. C.; Norris, M. R.; Templeton, J. L.; Meyer, T. J. *Inorg. Chem.* **2010**, *49*, 3980.

(9) Nagoshi, K.; Yagi, M.; Kaneko, M. *Bull. Chem. Soc. Jpn.* **2000**, *73*, 2193.
(10) Sens, C.; Romero, I.; Rodríguez, M.; Llobet, A.; Parella, T.; Benet-Buchholz, J. *J. Am. Chem. Soc.* **2004**, *126*, 7798.
(11) (a) Romain, S.; Bozoglian, F.; Sala, X.; Llobet, A. *J. Am. Chem. Soc.* **2009**, *131*, 2768. (b) Bozoglian, F.; Romain, S.; Ertem, M. Z.; Todorova, T. K.; Sens, C.; Mola, J.; Rodríguez, M.; Romero, I.; Benet-Buchholz, J.; Fontrodona, X.; Cramer, C. J.; Gagliardi, L.; Llobet, A. *J. Am. Chem. Soc.* **2009**, *131*, 15176.
(12) (a) Mola, J.; Mas-Marza, E.; Sala, X.; Romero, I.; Rodríguez, M.; Viñas, C.; Parella, T.; Llobet, A. *Angew. Chem., Int. Ed.* **2008**, *47*, 5830. (b) Francàs, L.; Sala, X.; Benet-Buchholz, J.; Escriche, L.; Llobet, A. *ChemSusChem* **2009**, *2*, 321.
(13) Zong, R.; Thummel, R. P. *J. Am. Chem. Soc.* **2005**, *127*, 12802.
(14) (a) Xu, Y.; Åkermark, T.; Gyollai, V.; Zou, D.; Eriksson, L.; Duan, L.; Zhang, R.; Åkermark, B.; Sun, L. *Inorg. Chem.* **2009**, *48*, 2717. (b) Xu, Y.; Duan, L.; Tong, L.; Åkermark, B.; Sun, L. *Chem. Commun.* **2010**, *46*, 6506.
(15) Wasylenko, D. J.; Ganesamoorthy, C.; Koivisto, B. D.; Berlinguette, C. P. *Eur. J. Inorg. Chem.* **2010**, *2010*, 3135.
(16) Wang, L.-P.; Wu, Q.; Van Voorhis, T. *Inorg. Chem.* **2010**, *49*, 4543.
(17) (a) Wada, T.; Tsuge, K.; Tanaka, K. *Angew. Chem., Int. Ed.* **2000**, *39*, 1479. (b) Muckerman, J. T.; Polyansky, D. E.; Wada, T.; Tanaka, K.; Fujita, E. *Inorg. Chem.* **2008**, *47*, 1787.
(18) Wada, T.; Muckerman, J. T.; Fujita, E.; Tanaka, K. *Dalton Trans.* **2011**, *40*, 2225.
(19) (a) Cape, J. L.; Hurst, J. K. *J. Am. Chem. Soc.* **2007**, *130*, 827. (b) Cape, J. L.; Siems, W. F.; Hurst, J. K. *Inorg. Chem.* **2009**, *48*, 8729.
(20) (a) Limburg, J.; Vrettos, J. S.; Liable-Sands, L. M.; Rheingold, A. L.; Crabtree, R. H.; Brudvig, G. W. *Science* **1999**, *283*, 1524. (b) Limburg, J.; Vrettos, J. S.; Chen, H.; de Paula, J. C.; Crabtree, R. H.; Brudvig, G. W. *J. Am. Chem. Soc.* **2000**, *123*, 423.
(21) Shimazaki, Y.; Nagano, T.; Takesue, H.; Ye, B.-H.; Tani, F.; Naruta, Y. *Angew. Chem., Int. Ed.* **2004**, *43*, 98.
(22) (a) Ferreira, K. N.; Iverson, T. M.; Maghlaoui, K.; Barber, J.; Iwata, S. *Science* **2004**, *303*, 1831. (b) Loll, B.; Kern, J.; Saenger, W.; Zouni, A.; Biesiadka, J. *Nature* **2005**, *438*, 1040. (c) Yano, J.; Kern, J.; Sauer, K.; Latimer, M. J.; Pushkar, Y.; Biesiadka, J.; Loll, B.; Saenger, W.; Messinger, J.; Zouni, A.; Yachandra, V. K. *Science* **2006**, *314*, 821. (d) Umena, Y.; Kawakami, K.; Shen, J.-R.; Kamiya, N. *Nature* **2011**, *473*, 55.
(23) (a) Concepcion, J. J.; Jurss, J. W.; Templeton, J. L.; Meyer, T. J. *J. Am. Chem. Soc.* **2008**, *130*, 16462. (b) Concepcion, J. J.; Jurss, J. W.; Norris, M. R.; Chen, Z.; Templeton, J. L.; Meyer, T. J. *Inorg. Chem.* **2010**, *49*, 1277.
(24) Concepcion, J. J.; Tsai, M.-K.; Muckerman, J. T.; Meyer, T. J. *J. Am. Chem. Soc.* **2010**, *132*, 1545.
(25) (a) Chen, Z.; Concepcion, J. J.; Jurss, J. W.; Meyer, T. J. *J. Am. Chem. Soc.* **2009**, *131*, 15580. (b) Concepcion, J. J.; Jurss, J. W.; Hoertz, P. G.; Meyer, T. J. *Angew. Chem., Int. Ed.* **2009**, *48*, 9473. (c) Chen, Z.; Concepcion, J. J.; Hull, J. F.; Hoertz, P. G.; Meyer, T. J. *Dalton Trans.* **2010**, *39*, 6950.
(26) (a) Chen, Z.; Concepcion, J. J.; Luo, H.; Hull, J. F.; Paul, A.; Meyer, T. J. *J. Am. Chem. Soc.* **2010**, *132*, 17670. (b) Chen, Z.; Concepcion, J. J.; Hu, X.; Yang, W.; Hoertz, P. G.; Meyer, T. J. *Proc. Natl. Acad. Sci. U.S.A.* **2010**, *107*, 7225.
(27) (a) Tseng, H.-W.; Zong, R.; Muckerman, J. T.; Thummel, R. *Inorg. Chem.* **2008**, *47*, 11763. (b) Zhang, G.; Zong, R.; Tseng, H.-W.; Thummel, R. P. *Inorg. Chem.* **2008**, *47*, 990.
(28) (a) Duan, L.; Fischer, A.; Xu, Y.; Sun, L. *J. Am. Chem. Soc.* **2009**, *131*, 10397. (b) Nyhlén, J.; Duan, L.; Åkermark, B.; Sun, L.; Privalov, T. *Angew. Chem., Int. Ed.* **2010**, *49*, 1773. (c) Tong, L.; Duan, L.; Xu, Y.; Privalov, T.; Sun, L. *Angew. Chem., Int. Ed.* **2011**, *50*, 445.
(29) (a) Duan, L.; Xu, Y.; Gorlov, M.; Tong, L.; Andersson, S.; Sun, L. *Chem.-Eur. J.* **2010**, *16*, 4659. (b) Li, L.; Duan, L.; Xu, Y.; Gorlov, M.; Hagfeldt, A.; Sun, L. *Chem. Commun.* **2010**, *46*, 7307.
(30) Roeser, S.; Farràs, P.; Bozoglian, F.; Martínez-Belmonte, M.; Benet-Buchholz, J.; Llobet, A. *ChemSusChem* **2011**, *4*, 197.
(31) Duan, L.; Xu, Y.; Tong, L.; Sun, L. *ChemSusChem* **2011**, *4*, 238.
(32) (a) Masaoka, S.; Sakai, K. *Chem. Lett.* **2009**, *38*, 182. (b) Yoshida, M.; Masaoka, S.; Sakai, K. *Chem. Lett.* **2009**, *38*, 702. (c) Yoshida, M.; Masaoka, S.; Abe, J.; Sakai, K. *Chem. Asian J.* **2010**, *5*, 2369.
(33) Kiyota, J.; Yokoyama, J.; Yoshida, M.; Masaoka, S.; Sakai, K. *Chem. Lett.* **2010**, *39*, 1146.
(34) (a) Wasylenko, D. J.; Ganesamoorthy, C.; Koivisto, B. D.; Henderson, M. A.; Berlinguette, C. P. *Inorg. Chem.* **2010**, *49*, 2202. (b) Wasylenko, D. J.; Ganesamoorthy, C.; Henderson, M. A.; Koivisto, B. D.; Osthoff, H. D.; Berlinguette, C. P. *J. Am. Chem. Soc.* **2010**, *132*, 16094. (c) Wadsworth, E.; Duke, F. R.; Goetz, C. A. *Anal. Chem.* **1957**, *29*, 1824.
(35) (a) McDaniel, N. D.; Coughlin, F. J.; Tinker, L. L.; Bernhard, S. *J. Am. Chem. Soc.* **2008**, *130*, 210. (b) Lalrempuia, R.; McDaniel, N. D.; Müller-Bunz, H.; Bernhard, S.; Albrecht, M. *Angew. Chem., Int. Ed.* **2010**, *49*, 9765.
(36) (a) Hull, J. F.; Balcells, D.; Blakemore, J. D.; Incarvito, C. D.; Eisenstein, O.; Brudvig, G. W.; Crabtree, R. H. *J. Am. Chem. Soc.* **2009**, *131*, 8730. (b) Blakemore, J. D.; Schley, N. D.; Balcells, D.; Hull, J. F.; Olack, G. W.; Incarvito, C. D.; Eisenstein, O.; Brudvig, G. W.; Crabtree, R. H. *J. Am. Chem. Soc.* **2010**, *132*, 16017.
(37) (a) Yang, X.; Baik, M.-H. *J. Am. Chem. Soc.* **2006**, *128*, 7476. (b) Yang, X.; Baik, M.-H. *J. Am. Chem. Soc.* **2008**, *130*, 16231.
(38) (a) Geletii, Y. V.; Botar, B.; Kögerler, P.; Hillesheim, D. A.; Musaev, D. G.; Hill, C. L. *Angew. Chem., Int. Ed.* **2008**, *47*, 3896. (b) Geletii, Y. V.; Besson, C.; Hou, Y.; Yin, Q.; Musaev, D. G.; Quiñonero, D.; Cao, R.; Hardcastle, K. I.; Proust, A.; Kögerler, P.; Hill, C. L. *J. Am. Chem. Soc.* **2009**, *131*, 17360. (c) Kuznetsov, A. E.; Geletii, Y. V.; Hill, C. L.; Morokuma, K.; Musaev, D. G. *J. Am. Chem. Soc.* **2009**, *131*, 6844. (d) Quiñonero, D.; Kaledin, A. L.; Kuznetsov, A. E.; Geletii, Y. V.; Besson, C.; Hill, C. L.; Musaev, D. G. *J. Phys. Chem. A* **2009**, *114*, 535.
(39) (a) Sartorel, A.; Carraro, M.; Scorrano, G.; Zorzi, R. D.; Geremia, S.; McDaniel, N. D.; Bernhard, S.; Bonchio, M. *J. Am. Chem. Soc.* **2008**, *130*, 5006. (b) Sartorel, A.; Miró, P.; Salvadori, E.; Romain, S.; Carraro, M.; Scorrano, G.; Valentin, M. D.; Llobet, A.; Bo, C.; Bonchio, M. *J. Am. Chem. Soc.* **2009**, *131*, 16051.
(40) (a) Geletii, Y. V.; Huang, Z.; Hou, Y.; Musaev, D. G.; Lian, T.; Hill, C. L. *J. Am. Chem. Soc.* **2009**, *131*, 7522. (b) Besson, C.; Huang, Z.; Geletii, Y. V.; Lense, S.; Hardcastle, K. I.; Musaev, D. G.; Lian, T.; Proust, A.; Hill, C. L. *Chem. Commun.* **2010**, *46*, 2784.
(41) (a) Orlandi, M.; Argazzi, R.; Sartorel, A.; Carraro, M.; Scorrano, G.; Bonchio, M.; Scandola, F. *Chem. Commun.* **2010**, *46*, 3152. (b) Puntoriero, F.; La Ganga, G.; Sartorel, A.; Carraro, M.; Scorrano, G.; Bonchio, M.; Campagna, S. *Chem. Commun.* **2010**, *46*, 4725. (c) Toma, F. M.; et al. *Nat. Chem.* **2010**, *2*, 826.
(42) (a) Yin, Q.; Tan, J. M.; Besson, C.; Geletii, Y. V.; Musaev, D. G.; Kuznetsov, A. E.; Luo, Z.; Hardcastle, K. I.; Hill, C. L. *Science* **2010**, *328*, 342. (b) Huang, Z.; Luo, Z.; Geletii, Y. V.; Vickers, J. W.; Yin, Q.; Wu, D.; Hou, Y.; Ding, Y.; Song, J.; Musaev, D. G.; Hill, C. L.; Lian, T. *J. Am. Chem. Soc.* **2011**, *133*, 2068.
(43) For the cobalt-based water oxidation catalysts, see: (a) Kanan, M. W.; Nocera, D. G. *Science* **2008**, *321*, 1072. (b) Surendranath, Y.; Dincă, M.; Nocera, D. G. *J. Am. Chem. Soc.* **2009**, *131*, 2615. (c) Kanan, M. W.; Yano, J.; Surendranath, Y.; Dincă, M.; Yachandra, V. K.; Nocera, D. G. *J. Am. Chem. Soc.* **2010**, *132*, 13692. (d) McAlpin, J. G.; Surendranath, Y.; Dincă, M.; Stich, T. A.; Stoian, S. A.; Casey, W. H.; Nocera, D. G.; Britt, R. D. *J. Am. Chem. Soc.* **2010**, *132*, 6882.
(44) (a) Sadakane, M.; Higashijima, M. *Dalton Trans.* **2003**, 659. (b) Sadakane, M.; Tsukuma, D.; Dickman, M. H.; Bassil, B.; Kortz, U.; Higashijima, M.; Ueda, W. *Dalton Trans.* **2006**, 4271.
(45) The pH dependence of **1** with more limited pH region was reported in ref 44a.
(46) No observation of catalytic currents at the highest anodic peak in Figure 3 is consistent with the rate-determining step in Scheme 1, which is not the oxidation of the catalyst. The cathodic scan from the potential higher than 1.1 V vs SCE with slow scan rate (50 mV s^{-1}) resulted in the catalytic current for the water oxidation, which increases with increasing concentration of the catalyst (see Figure S6 in the Supporting Information).

(47) Pourbaix, M. *Atlas of Electrochemical Equilibria in Aqueous Solutions*; NACE: Houston, 1966.
(48) Dobson, J. C.; Meyer, T. J. *Inorg. Chem.* **1988**, *27*, 3283.
(49) (a) Mullay, J. *J. Am. Chem. Soc.* **1984**, *106*, 5842. (b) Allen, L. C. *J. Am. Chem. Soc.* **1989**, *111*, 9003.
(50) The lower limit of the time scale of stopped-flow measurements is about 10 ms due to the mixing of two solutions. When the reactive species decays obeying the first-order kinetics and its half-life period is longer than 10 ms, the first-order rate constant must be less than ca. 10^2 s^{-1} for the determination of the rate constant using a stopped-flow apparatus. As the concentration of catalyst **1** must be higher than ca. 10^{-4} M because of the detectable limit of the absorbance change ($\Delta A \approx$ ca. 0.1), the second-order rate constant must be lower than 10^6 M^{-1} s^{-1} ($=10^2$ $s^{-1}/10^{-4}$ M) for the accurate determination of the rate constant.
(51) (a) Medhi, O. K.; Agarwala, U. *Inorg. Chem.* **1980**, *19*, 1381. (b) Taqui Khan, M. M.; Srinivas, D.; Kureshy, R. I.; Khan, N. H. *Inorg. Chem.* **1990**, *29*, 2320. (c) Besson, C.; Mirebeau, J.-H.; Renaudineau, S.; Roland, S.; Blanchard, S.; Vezin, H.; Courillon, C.; Proust, A. *Inorg. Chem.* **2011**, *50*, 2501. (d) Sukanya, D.; Raja, D. S.; Bhuvanesh, N. S. P.; Natarajan, K. *Polyhedron* **2011**, *30*, 1108. (e) Mondal, B.; Chakraborty, S.; Munshi, P.; Walawalkar, M. G.; Lahiri, G. K. *J. Chem. Soc., Dalton Trans.* **2000**, 2327.
(52) (a) Dengel, A. C.; Griffith, W. P.; O'Mahoney, C. A.; Williams, D. J. *J. Chem. Soc., Chem. Commun.* **1989**, 1720. (b) Dengel, A. C.; Griffith, W. P. *Inorg. Chem.* **1991**, *30*, 869. (c) Neumann, R.; Abu-Gnim, C. *J. Am. Chem. Soc.* **1990**, *112*, 6025. (d) Lahootun, V.; Besson, C.; Villanneau, R.; Villain, F.; Chamoreau, L.-M.; Boubekeur, K.; Blanchard, S.; Thouvenot, R.; Proust, A. *J. Am. Chem. Soc.* **2007**, *129*, 7127. (e) Kuan, S. L.; Tay, E. P. L.; Leong, W. K.; Goh, L. Y.; Lin, C. Y.; Gill, P. M. W.; Webster, R. D. *Organometallics* **2006**, *25*, 6134.
(53) Sidorenko, A. V.; Rodnyĭ, P. A.; Guillot-Noel, O.; Gourier, D.; van Eijk, C. W. E. *Phys. Solid State* **2003**, *45*, 1676.
(54) Hunt, J. K.; Zhou, J.; Lei, Y. *Inorg. Chem.* **1992**, *31*, 1010.
(55) Yamada, H.; Hurst, J. K. *J. Am. Chem. Soc.* **2000**, *122*, 5303.
(56) The effect of ionic strength was examined by the addition of 0.5 M $NaNO_3$ to the solution of 0.1 M HNO_3 (pH 1), and it was confirmed that neither the rate constant nor the pH of the solution was affected by the ionic strength.
(57) The more electronegative Ge withdraws electron at higher degree than Si from the framework of polytungstate anion, which causes the lower basicity of the heteropolytungstate anion. The weaker coordination of the heteropolytungstate anion resulted in the higher acidity of the Ru metal center, which induces the higher acidity of the coordinated aqua ligand with lower pK_a as well as the higher electrophilicity of the Ru metal center appropriate for the rate-determining nucleophilic attack of a water molecule to the Ru center.